Title

Broadcasting of amplitude- and frequency-modulated c-di-GMP signals facilitates cooperative surface commitment in bacterial lineages

Journal

Proceedings of the National Academy of Sciences of the United States of America, 119(4)

ISSN

0027-8424

Authors

Lee, Calvin K
Schmidt, William C
Webster, Shanice S
et al.

Publication Date

2022-01-25

DOI

10.1073/pnas.2112226119

Peer reviewed

Broadcasting of amplitude- and frequency-modulated c-di-GMP signals facilitates cooperative surface commitment in bacterial lineages

Calvin K. Lee[a,b,c], William C. Schmidt[a,b,c], Shanice S. Webster[d], Jonathan W. Chen[a,b,c], George A. O'Toole[d], and Gerard C. L. Wong[a,b,c,1]

[a]Department of Bioengineering, University of California, Los Angeles, CA 90095; [b]Department of Chemistry and Biochemistry, University of California, Los Angeles, CA 90095; [c]California NanoSystems Institute, University of California, Los Angeles, CA 90095; and [d]Department of Microbiology and Immunology, Geisel School of Medicine at Dartmouth, Hanover, NH 03755

Edited by Knut Drescher, Biozentrum, Max-Planck-Institut fur terrestrische Mikrobiologie, Basel, Switzerland; received July 2, 2021; accepted November 22, 2021 by Editorial Board Member Daan Frenkel

Work on surface sensing in bacterial biofilms has focused on how cells transduce sensory input into cyclic diguanylate (c-di-GMP) signaling, low and high levels of which generally correlate with high-motility planktonic cells and low-motility biofilm cells, respectively. Using Granger causal inference methods, however, we find that single-cell c-di-GMP increases are not sufficient to imply surface commitment. Tracking entire lineages of cells from the progenitor cell onward reveals that c-di-GMP levels can exhibit increases but also undergo oscillations that can propagate across 10 to 20 generations, thereby encoding more complex instructions for community behavior. Principal component and factor analysis of lineage c-di-GMP data shows that surface commitment behavior correlates with three statistically independent composite features, which roughly correspond to mean c-di-GMP levels, c-di-GMP oscillation period, and surface motility. Surface commitment in young biofilms does not correlate to c-di-GMP increases alone but also to the emergence of high-frequency and small-amplitude modulation of elevated c-di-GMP signal along a lineage of cells. Using this framework, we dissect how increasing or decreasing signal transduction from wild-type levels, by varying the interaction strength between PilO, a component of a principal surface sensing appendage system, and SadC, a key hub diguanylate cyclase that synthesizes c-di-GMP, impacts frequency and amplitude modulation of c-di-GMP signals and cooperative surface commitment.

bacteria biofilms | *Pseudomonas aeruginosa* | surface sensing | cyclic-di-GMP | motility

Surface sensing is a pivotal step in bacterial biofilm formation. For example, work on initial stages of surface sensing in *Pseudomonas aeruginosa* has focused on how single cells transduce sensory input into cyclic diguanylate (c-di-GMP) signaling, either indirectly through cyclic AMP (cAMP) induction via the Pil-Chp machinery (1–4) or directly via the Wsp system (5–9). In multiple bacteria species, the broadly accepted model is that low c-di-GMP levels correlate with high-motility, free-swimming planktonic cells, whereas high c-di-GMP levels correlate with low-motility, sessile cells with elevated levels of exopolysaccharide (EPS) biosynthesis (10–24). It is not known whether increased c-di-GMP levels constitute a necessary or sufficient condition for surface commitment: That increased c-di-GMP correlates with increased tendency for biofilm formation seems to be an overall trend that holds true, but there have also been many observed exceptions to this model, especially at the single-cell level. Recent work suggests that these exceptions are a natural consequence of surface sensing, and not merely a matter of statistics or measurement error (4, 9, 25). Furthermore, the well-studied biofilm-forming bacterial species have a rich diversity of diguanylate cyclases (DGCs) and phosphodiesterases (PDEs) for producing and degrading c-di-GMP, and how these specific enzymes function as part of a larger second messenger signaling network in the context of surface sensing remains a challenging problem. A natural question to ask is what happens after detection of a surface has been established via increased c-di-GMP–based surface sensing in single cells of *P. aeruginosa* PA14 (PA14), but before collective surface commitment by a cell population.

Using Granger causal inference methods, we find that c-di-GMP increases at the single-cell level are not sufficient to establish a causal link to surface commitment. Tracking the temporal progression of entire lineages of PA14 cells from the progenitor cell onward for 10 to 20 generations reveals that c-di-GMP levels do not exhibit monotonic increases but rather undergo oscillations with periods of several division times (periods ranging from 2 to 20 h, with division times of ∼1 h). To assess whether these c-di-GMP oscillations are important or not for biofilm formation, we use principal component analysis (PCA) and factor analysis (FA) to see how lineage-level c-di-GMP data correlate with surface commitment of the lineage, quantified by how many cells of a given lineage stay on the surface, by the architecture of the family trees, and by whether the entire lineage detaches or not.

Significance

It is well known that c-di-GMP concentration rises in surface-sensing bacteria and functions as a "molecular switch" for biofilm formation. Here, we provide an important recasting of this picture: Intracellular c-di-GMP signals do not just increase in surface-sensing bacteria; such signals are cooperatively broadcast across multiple generations of cells in a lineage with oscillations that undergo both amplitude and frequency modulation, which are controlled by the coupling between pili appendages and c-di-GMP synthesis machinery. The right "tuning" of these signals in terms of frequency and amplitude correlates ultimately to surface commitment. Amplitude and frequency modulation of c-di-GMP signals allows encoding of more complex instructions. Thus, our work provides a more nuanced understanding of how c-di-GMP signaling drives surface commitment.

Author contributions: C.K.L., G.A.O., and G.C.L.W. designed research; C.K.L. and W.C.S. performed research; C.K.L., W.C.S., S.S.W., J.W.C., and G.A.O. contributed new reagents/analytic tools; C.K.L., W.C.S., and J.W.C. analyzed data; C.K.L., G.A.O., and G.C.L.W. wrote the paper; and C.K.L., W.C.S., S.S.W., J.W.C., G.A.O., and G.C.L.W. contributed feedback and discussion.

The authors declare no competing interest.

This article is a PNAS Direct Submission. K.D. is a guest editor invited by the Editorial Board.

[1]To whom correspondence may be addressed. Email: gclwong@seas.ucla.edu.

This article contains supporting information online at http://www.pnas.org/lookup/suppl/doi:10.1073/pnas.2112226119/-/DCSupplemental.

Published January 21, 2022.

Surprisingly, the results suggest that successful surface commitment is not due to elevated c-di-GMP levels alone but also to the ability of cells' c-di-GMP regulatory machinery to cooperatively transform initial c-di-GMP signal increases induced by surface sensing into an amplitude- and frequency-modulated oscillatory signal that propagates across multiple generations in a lineage of cells. To test this idea, we demonstrate how adjusting the strength of PilO–SadC interactions or deleting the *sadC* gene can impact modulation of c-di-GMP oscillations and resultant downstream surface commitment, and we show that this approach directly tracks not just how the activity of a key surface-sensing appendage (type 4 pili [T4P]) is transduced into the activity of a surface sensing DGC but also how this process is influenced by the rest of the cell's c-di-GMP regulatory machinery.

Results

C-di-GMP Levels in Lineages of Bacteria Undergo Multigenerational Oscillations. To observe the levels of c-di-GMP in single cells in flow cell experiments we utilize a fluorescence reporter previously described (26), wherein green fluorescent protein (GFP) is fused to the c-di-GMP–responsive P_{cdrA} promoter. We used this reporter system to interrogate the relationship between c-di-GMP levels and whether a cell will detach from the surface. In these experiments, for cells where we specifically observed a detachment event, we label them as "detach." Otherwise, we label cells where we did not observe a detachment event as "persist." Using these categories, we first look at the last observed c-di-GMP level at the time of the given event. Surprisingly, we readily observe all possible combinations, where cells can detach or persist with either high or low c-di-GMP levels (Fig. 1). The cases corresponding to cells detaching with low c-di-GMP and persisting with high c-di-GMP are more common, but the other cases corresponding to cells detaching with high c-di-GMP and persisting with low c-di-GMP are not rare. In fact, we observe the c-di-GMP levels to span a large range for both cells that persist or detach (Fig. 1*E*). With sufficient measurement statistics, the mean c-di-GMP signal of the persisting cells can be shown to be slightly but significantly higher than the detaching cells, but the effect size of this difference is surprisingly small (i.e., the difference in the average value is smaller than the spread of the distribution), suggesting that it is difficult to correlate a detachment event with the c-di-GMP level at a single-cell level at the time of the persist/detach event.

Since c-di-GMP changes are subtle for single cells within a single division cycle, we track many cells longitudinally to gain more information from a larger perspective. Specifically, we track lineages of cells, starting with the founder cell that lands on the surface and following its progeny on the surface over time and multiple division events. By doing this analysis, we observe that the c-di-GMP levels in these lineages undergo oscillations over several division generations, with the lineages having an average division time of ∼1 h (*SI Appendix*, Fig. S1). Oscillations are present in nearly every tracked lineage (Fig. 2), so long as that lineage is long enough for an oscillation to be observed (i.e., can see at least half of a cycle), which corresponds to at least three to four division generations.

Lineages That Persist Correlate with c-di-GMP Levels That Are Elevated and Oscillating with Short Oscillation Periods. With this analysis, we now have enough data with high time resolution and span to apply causal inference techniques to determine how increases in c-di-GMP relate to surface commitment. To do so, we need additional quantitative measurements of surface commitment that have the same temporal resolution and span as the c-di-GMP measurements. One such measurement is the number of cells in a lineage, which makes intuitive sense, since a lineage with more progeny is more likely to commit to the surface, and vice versa. To assess the relationship between c-di-GMP levels and the number of cells in a lineage we utilized Granger causality (G-causality). G-causality (27) is a statistical formulation of predictive causality based on measuring the ability of a signal to predict an outcome, one that has been used broadly in economics and neuroscience. When we apply G-causality on c-di-GMP versus the number of cells in a lineage, we find that most data have nonsignificant probabilities of G-causality between the time-series data of c-di-GMP levels and number of cells in a lineage. This finding suggests that in addition to intracellular c-di-GMP levels, additional experimentally measured parameters are needed before the collective dataset can reliably correlate with surface commitment by cells in a lineage.

To quantify and assess the degree to which a combination of multiple measured parameters can reliably correlate with surface commitment, we next use PCA and FA, which are common descriptive statistical techniques used to reveal underlying correlations. To perform this analysis, we first extract relevant features from the lineage time-series data. The features used in this analysis are described below.

We use two measured quantities to characterize surface commitment for lineages. The first measurement is an extension of the "persist" vs. "detach" categories described earlier for single cells to lineages. Here, we label a lineage as "detach" if the final generation of progeny all undergo a detachment event; otherwise, a lineage is labeled as "persist" if at least one of the descendants persists (*SI Appendix*, Fig. S2). For the second measured quantity, we utilize a variation of the tree asymmetry parameter we previously described (4). In brief, tree asymmetry Λ_a is an order parameter that characterizes the overall architecture of a binary tree. Since bacteria divide into two, lineages are effectively a binary tree, so this parameter can be applied. To have this parameter characterize surface persistence, we utilize $1-\Lambda_a$ (which we denote as tree symmetry Λ_s), so that a larger tree symmetry value corresponds to a larger portion of a lineage persisting on the surface: $\Lambda_s = 0$ corresponds to a perfectly "one-legged" family tree, where only one of the two daughter cells stays on the surface after division; $\Lambda_s = 1$ corresponds to a perfectly "two-legged" family tree, where both daughter cells stay on the surface after division.

Next, for c-di-GMP time series we calculate parameters that characterize an oscillation, which include the mean (or baseline), the amplitude, and the period (or frequency). We first extract a c-di-GMP time-series trace for each lineage, where multiple cells in a lineage present at a single time point are averaged together. These time-series data are then fit, via two different methods, to a sine function $C(t) = A_0 + A_1 \sin\left(\frac{2\pi t}{T} - T_0\right)$, where A_0 is the mean, A_1 is the amplitude, T is the period, and T_0 is the phase of the sine function (Fig. 2). The blue lines represent the first fit method, where the fit is performed to find all the coefficients $[A_0, A_1, T, T_0]$. The red lines represent the second fit method, where certain coefficients are substituted with values calculated from the time series data before performing the fit: A_0 is substituted with the mean of the time series data; A_1 is substituted with a multiple of the variance of the time series data (so $A_1 = A * var$); and T is substituted with the period of the time-series data, which is calculated as follows. The power spectral density (via Lomb–Scargle periodogram) estimate is calculated from the time series, which provides weights to each frequency (or 1/period), which is then used to calculate a weighted average period. After substituting the previously described values, the fit is then performed to find the coefficients $[A, T_0]$. Comparing the two fit methods, which provide similar results but have different degrees of freedom, reveals interesting features of the oscillatory characteristics of the data. For example, the amplitude of the oscillation (which generally requires the time structure to calculate) is related to the variance of the time

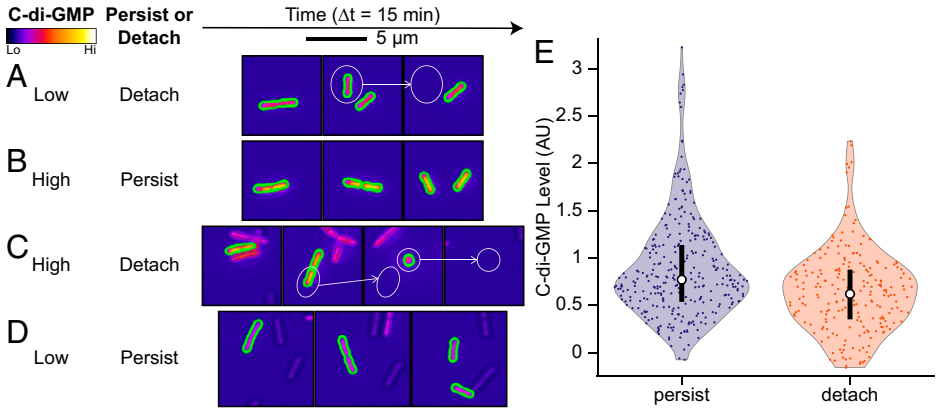

Fig. 1. Cells can persist or detach with either high or low c-di-GMP levels. Events where (*A*) a cell detaches (note the white arrow and circle) with low c-di-GMP and (*B*) a cell persists with high c-di-GMP are common. However, the other cases where (*C*) a cell detaches with high c-di-GMP and (*D*) a cell persists with low c-di-GMP are not rare. All four combinations are readily observable in the dataset. (*E*) Quantification of the last observed c-di-GMP levels at the time of the "detach" or "persist" event. In these violin plots, the points represent individual data points, the circles represent the median, and the lines represent the IQR (25th to 75th percentiles). Bootstrap sampling of the medians of the two distributions shows that they are statistically significantly different (P < 1e-3). However, the difference between the medians (0.15) is smaller than the IQR (0.58 for "persist" and 0.51 for "detach"), suggesting that this difference is difficult to observe due to having an effect size that is not large. For "detach" events, it is very common for cells to detach after dividing but before the fluorescence imaging interval of 15 min, so in these cases the last known c-di-GMP level of the mother cell is used.

series data (which is a calculation that does not depend on the time structure) by a constant factor.

Finally, previous work has shown that single-cell surface motility is another important component related to biofilm formation and surface commitment (4, 9, 25, 28–30). As a result, we measure parameters that characterize surface motility, such as the radius of gyration of the trajectory and its mean squared displacement (MSD) slope. These motility parameters are calculated from the positional tracking data, where we extract a trajectory for each lineage and multiple cells in a lineage present at a single time point have their positions averaged together. The radius of gyration measures the spatial extent, or "spread," of the trajectory (i.e., how much surface is traversed), and the MSD slope measures the directionality of the trajectory (i.e., how straight the trajectory is).

In order to identify potential behavioral differences between different branches in a lineage of cells, we consider two types of data entities: lineages and branches (*SI Appendix*, Fig. S2). In the former, we treat the entire lineage, including the founder cell and all its surface progeny, as a single entity. In the latter, we treat each branch of a lineage (i.e., following the lineage from the founder cell to a single daughter cell after each division event) as a single entity. As a result, the branch data also implicitly contain information on how cells are related through division events (e.g., siblings and parents). Both methods are representations of the underlying intricate lineage tree data containing all the different generational relations (e.g., "cousins," "grandchildren," and "grandparents") and offer distinct but complementary insights into the data. For example, multiple related cells in a lineage present at the same time point are combined for lineage data but are held separate for branch data. Both methods incorporate the longitudinal multigenerational history of the cell as a key feature. It is interesting to see whether these methods will provide similar or different results, which yield information on how well cellular behavior for different branches correlates with the average behavior of a lineage.

We use the following experimentally derived parameters as input variable to the analysis: tree symmetry (TreeSym), c-di-GMP mean (Mean), c-di-GMP amplitude (Amplitude), c-di-GMP period (Period), radius of gyration (RadOfGyr), and MSD slope (MSD). We then utilize PCA and FA to see how these multiple inputs relate to surface commitment. Importantly, we find that the data can be reduced to three independent dimensions via PCA while still explaining roughly 70 to 90% of the variance in the data (*SI Appendix*, Fig. S4). To better see what these three dimensions correspond to in terms of the above input variables that characterize surface commitment, c-di-GMP, and motility, we perform FA using the varimax rotation, which can better align the dimensions, or factors, with the variables (to make the output more interpretable) at the cost of lowering the overall explained variance (from 85 to 90% to 65 to 70%). The resulting rotated factor loadings and variance explained per dimension from FA are seen in Fig. 3, while the original unrotated variance explained and coefficients per dimension from PCA are seen in *SI Appendix*, Fig. S4. Each dimension in FA is named by the variable that has the largest factor loading in that dimension. In other words, one dimension is dominated by the mean c-di-GMP, one by the c-di-GMP oscillation period, and one by the surface motility. Furthermore, these three dimensions are by construction orthogonal to each other, which indicates that these dimensions are statistically independent of each other in their contribution to describing surface commitment. We are now in a good position to investigate how each dimension (mean c-di-GMP levels, c-di-GMP period, and bacterial motility) quantitatively correlates with surface commitment.

The dimension corresponding to c-di-GMP mean is the largest component that explains roughly one-third of the total variance, and the results for this dimension are similar when using lineage or branch data (Fig. 3 *A* and *D*). Tree symmetry has a large positive factor loading in this dimension, which suggests that this dimension has a strong positive correlation with surface commitment. We can see this directly in the data as well. For both lineages and branches, tree symmetry has a positive Spearman correlation with c-di-GMP mean ($\rho = 0.59$, $P = 0.00083$ for lineages; $\rho = 0.57$, $P < 0.0001$ for branches), which indicates that lineages that have a larger fraction of their progeny persist on the surface tend to have a higher c-di-GMP mean. This observation is consistent with our present understanding of c-di-GMP and its effects. Interestingly, in this dimension, c-di-GMP amplitude also has a large positive factor loading, which implies the same scenario. However, tree symmetry has a lower Spearman correlation with c-di-GMP amplitude ($\rho = 0.14$, $P = 0.46$ for lineages; $\rho = 0.36$, $P < 0.0001$ for branches), which implies that correlation between these two parameters is not strong. Instead, we find that c-di-GMP amplitude has a positive Spearman correlation with c-di-GMP mean ($\rho = 0.51$, $P = 0.0054$ for lineages;

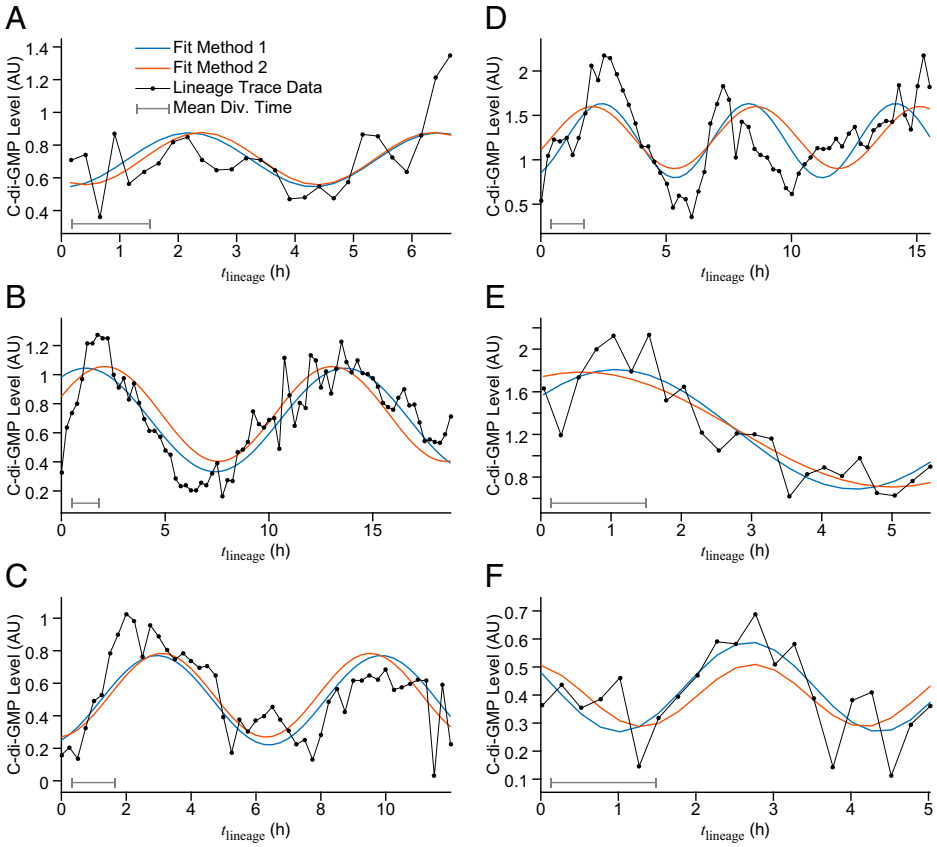

Fig. 2. By tracking c-di-GMP levels for longer periods of time in lineages we find that c-di-GMP levels have oscillatory behavior over several division generations. (*A–F*) Shown are six different lineages tracked over the indicated time. Gray lines in the bottom left corner of the plots denote the mean division time in a lineage (~1 h). Black points and lines denote the lineage trace data for c-di-GMP, where each point represents one time point and multiple cells in a lineage present at a single time point are averaged together. This time-series data are then fit, via two different methods, to a sine function $C(t) = A_0 + A_1 \sin\left(\frac{2\pi t}{T} - T_0\right)$, where A_0 is the mean, A_1 is the amplitude, T is the period, and T_0 is the phase of the sine function. The blue lines represent the first fit method, where the fit is performed to find all the coefficients [A_0, A_1, T, T_0]. The red lines represent the second fit method, where certain coefficients are substituted with values calculated from the time-series data before performing the fit: A_0 is substituted with the mean of the time-series data; A_1 is substituted with a multiple of the variance of the time series data (so $A_1 = A * var$); and T is substituted with the period of the time-series data, which is calculated as follows. The power spectral density (via Lomb–Scargle periodogram) estimate is calculated from the time series, which provides weights to each frequency (or 1/period), which is then used to calculate a weighted average period. After substituting the previously described values, the fit is then performed to find the coefficients [A, T_0]. Both fit methods provide similar results but have different degrees of freedom. Each plot in *A–F* is a different strain, summarized along with the fit coefficients in *SI Appendix*, Table S1. For each plot, the scale is set such that the oscillatory shape of the curve is easily visible. The same plots using a unified scale is shown in *SI Appendix*, Fig. S3.

$\rho = 0.77$, $P < 0.0001$ for branches), which indicates that lineages that have a higher c-di-GMP mean will tend to have a higher c-di-GMP amplitude (i.e., larger fluctuations in the c-di-GMP levels over time for larger mean values of c-di-GMP). This correlation agrees with previous results (31), since the amplitude is directly related to the variance of the time series. From these results, we see that c-di-GMP mean correlates positively with surface commitment, which agrees with the general trend of how elevated c-di-GMP levels correlate with biofilm formation. However, this correlation is only part of the whole picture since we are incorporating the entire history of a lineage into the c-di-GMP mean. We also find that larger c-di-GMP means directly correlate with larger fluctuations in the c-di-GMP signal, which implies that fluctuations are an important component of c-di-GMP signaling and surface commitment. Furthermore, because both the lineage and branch data show similar results, this finding indicates that individual members of the lineage will also have a similar behavior. Thus, it is not just the c-di-GMP history of a specific cell but rather the entire history of c-di-GMP levels of its ancestors that contributes to their surface commitment behavior.

The two dimensions corresponding to c-di-GMP period and surface motility are the next largest and each explains roughly 20% of the total variance (roughly two-thirds of the effect from mean c-di-GMP levels; Fig. 3 *B*, *C*, *E*, and *F*). In both of these dimensions, c-di-GMP mean and amplitude have relatively small factor loadings, and c-di-GMP period and surface motility also have small factor loadings in the dimension corresponding to c-di-GMP mean, which implies that c-di-GMP period and surface motility are separate contributions to surface commitment from c-di-GMP mean and amplitude. In both dimensions, we find that tree symmetry has a negative factor loading for both lineages and branches, which suggests that both c-di-GMP period and surface motility have a negative correlation with surface commitment. However, the magnitude of the factor loading is smaller for branches, which suggests that these effects are more prominent when considering the entire lineage rather than only individual members of the lineage as a single entity. This result is interesting: Rather than having these effects "wash out" by averaging across different branches of a lineage, they actually combine to give a stronger effect, which implies that the behavior of an entire lineage is more correlated than expected.

A negative factor loading for tree symmetry in the dimension corresponding to c-di-GMP period indicates that lineages that are more likely to be surface-committed tend to have shorter

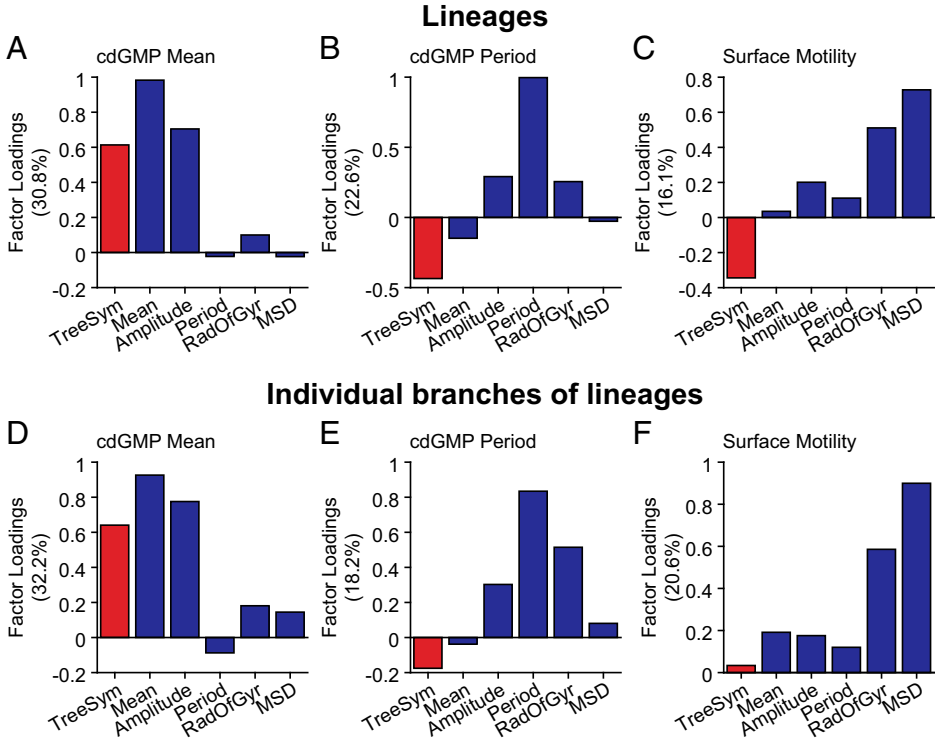

Fig. 3. Factor analysis (FA) reveals three orthogonal dimensions of data: c-di-GMP mean, c-di-GMP period, and surface motility. Each dimension contributes independently to surface commitment and is named by the variable that has the largest factor loading in that dimension. Tree symmetry is one quantitative indicator of surface commitment (e.g., a larger tree symmetry value corresponds to a larger portion of a lineage committing to the surface), so the factor loading of tree symmetry (red bars) in each dimension can indicate how that dimension contributes to surface commitment. Analysis is applied to lineage data in *A*–*C* as well as individual branch data in *D*–*F*. (*A* and *D*) This dimension corresponds to c-di-GMP mean (and c-di-GMP amplitude) and explains ∼31 to 32% of the variance in the data for both lineages and branches. Tree symmetry has a positive factor loading in this dimension for both lineages and branches, which suggests that this dimension has a positive correlation with surface commitment (i.e., larger c-di-GMP mean correlates with higher surface commitment). (*B* and *E*) This dimension corresponds to c-di-GMP period and explains ∼18 to 23% of the variance in the data for both lineages and branches. At the lineage level, tree symmetry has a negative factor loading, which suggests that this dimension has a negative correlation with surface commitment (i.e., shorter c-di-GMP period correlates with higher surface commitment). However, at the branch level, tree symmetry has a negative factor loading with a smaller magnitude, which suggests that there is reduced correlation with surface commitment. (*C* and *F*) This dimension corresponds to surface motility (MSD slope and radius of gyration) and explains ∼16% and ∼21% of the variance in the data for lineages and branches, respectively. At the lineage level, tree symmetry has a negative factor loading, which suggests that this dimension has a negative correlation with surface commitment (i.e., lower surface motility correlates with higher surface commitment). However, at the branch level, tree symmetry has a factor loading close to zero, which suggests that there is little correlation with surface commitment.

periods and thus can control their c-di-GMP levels within a narrower "window" by not allowing prolonged increases or decreases. We also see a negative Spearman correlation between c-di-GMP period and tree symmetry for lineages ($\rho = -0.45$, $P = 0.013$ for lineages; $\rho = -0.17$, $P = 0.00012$ for branches). A negative factor loading for tree symmetry in the dimension corresponding to surface motility indicates that lineages that are more likely to be surface committed tend to have lower surface motility, consistent with previous findings (32–35). For lineages, radius of gyration has a negative Spearman correlation with tree symmetry ($\rho = -0.39$, $P = 0.036$), but MSD slope does not ($\rho = -0.13$, $P = 0.50$). These results indicate that lineages that are more surface committed tend to traverse a smaller portion of the surface but do not change their preference for which direction they tend to traverse. For branches, both measured motility parameters have little Spearman correlation with tree symmetry ($\rho = -0.0018$, $P = 0.97$ for radius of gyration; $\rho = 0.071$, $P = 0.10$ for MSD slope).

Together, from these results we find additional factors, beyond just the c-di-GMP mean, that contribute to surface commitment. In particular, we find that c-di-GMP has an additional independent contribution to surface commitment in the form of the oscillation period, which implies that the oscillatory behavior of the c-di-GMP signal is an important feature for surface commitment. Similarly, surface motility is a contributing factor. Here, we again find that these factors are similar between lineage and branch data but more prominent in the lineage data despite a greater degree of averaging. This observation suggests that surface commitment behavior of individual branches reflects the collective surface commitment behavior of the full lineage.

Similar results can be seen when using whether a lineage will detach or persist as an indicator of surface commitment compared with using tree symmetry, which is interesting because these two experimentally derived parameters measure completely different aspects of surface commitment for lineages. Tree symmetry quantifies the fraction of individual branch surface commitment behavior, whereas a lineage detaching or persisting describes the collective surface commitment behavior of the entire lineage. For example, a lineage can persist but have a daughter cell detach every generation, which will have a tree symmetry value close to zero. Conversely, a lineage can have the final generation of its progeny detach even though progeny in prior generations persist, which will have a tree symmetry value close to one. We categorize factor scores, which are the data points for each factor or dimension, by whether that lineage detaches or persists and plot the results in Fig. 4. We find that lineages that persist (i.e., higher surface commitment) tend to have higher c-di-GMP mean (Fig. 4*A*), shorter c-di-GMP period (Fig. 4*B*), and lower surface motility (Fig. 4*C*) compared

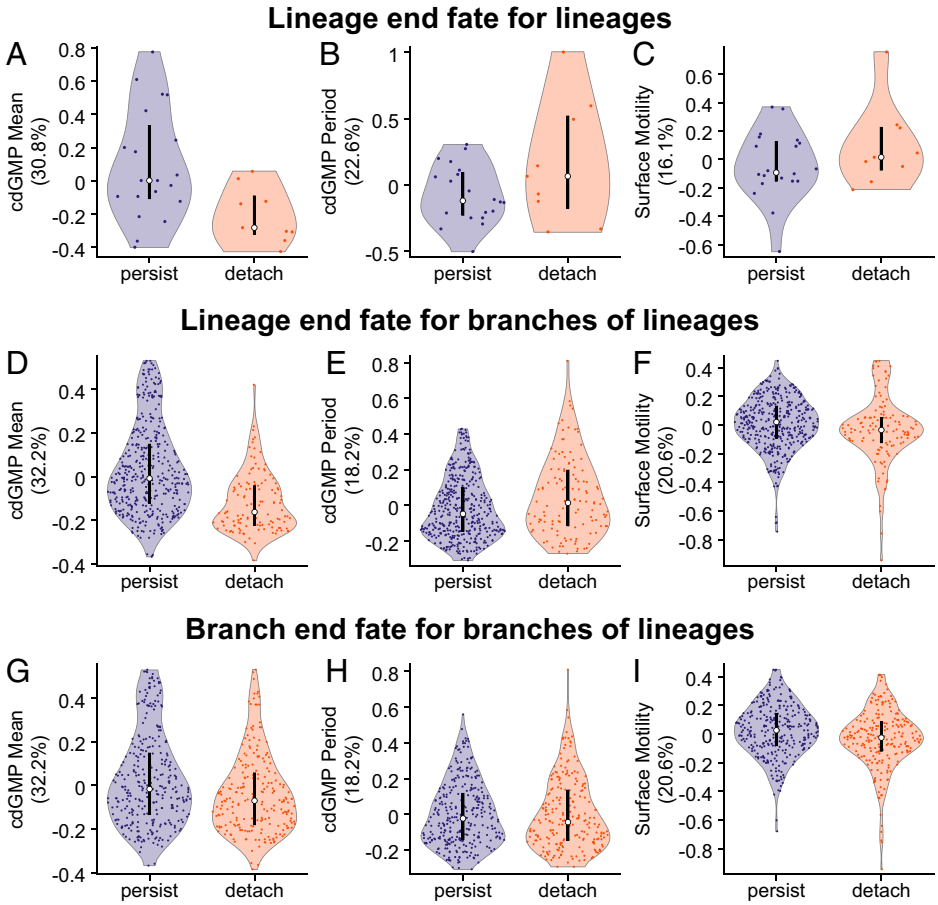

Fig. 4. Lineages that persist tend to have a larger c-di-GMP mean, less surface motility, and a shorter c-di-GMP period compared with lineages that detach. Lineage end fate is where a lineage either persists or detaches, while branch end fate is where an individual branch either persists or detaches. These end fates are also indicators of surface commitment, as they directly relate to whether a cell or lineage will commit to the surface or not. Each data point in *A–C* corresponds to one lineage, while each data point in *D–I* corresponds to one branch in the lineage. Differences in persisting vs. detaching for each dimension are greatest when using lineage data and reduced when using branch data, suggesting that surface commitment depends more on the long-term, collective behavior of the lineage rather than on the behavior of individual members.

with lineages that detach (i.e., lower surface commitment). The trends between detaching or persisting are harder to differentiate when using branch data (Fig. 4 *D–I*). The results here using factor scores and whether a lineage will detach or persist agree with the results in Fig. 3 and *SI Appendix*, Fig. S4 on the factor loadings and tree symmetry. In other words, statistical analysis of these longitudinal data shows the surprising result that different individual branches of the family tree are not independent but rather correlated with the entire lineage in terms of surface commitment. Furthermore, factors other than mean c-di-GMP impact whether individual bacteria persist or detach.

PilO–SadC Interactions Facilitate Surface Commitment by Amplitude and Frequency Modulation of c-di-GMP Oscillations in a Lineage of Cells. Previous work on one of the known c-di-GMP signaling system in *P. aeruginosa*, which involves the SadC DGC and the T4P complex, has shown that PilO, one of the proteins in the T4P complex, can physically interact with SadC and that PilO–SadC interaction inhibits SadC's activity (31). From the present analysis, we now have an augmented profiling framework for identifying lineages that are in the process of surface commitment, which in young biofilms correlates with the structure of the family tree (via the tree symmetry parameter) and whether a lineage will detach or persist. The profiling framework is based on three dimensions or composite features, each based on multiple parameters: one feature based mostly on mean c-di-GMP levels (accounting for 31 to 32% of the total variance of the data), one mostly on the period of c-di-GMP oscillations (18 to 23%), and one mostly on bacterial surface motility (16 to 21%). It is important to note that these three features are statistically independent in their contribution to describing whether a lineage is likely to be surface-committed or not. Lineages that are more likely to be surface-committed (i.e., tree symmetry value closer to one or the lineage persists) tend to have higher mean c-di-GMP levels, shorter c-di-GMP oscillation periods, and lower surface motility compared with lineages that are less likely to be surface-committed (i.e., tree symmetry value closer to zero or the lineage detaches). We can apply this framework to visualize how PilO–SadC interactions and related signal proteins impact c-di-GMP signaling and the resultant process of surface commitment in young biofilms. We categorize the factor scores by the interaction strength type: the increased PilO–SadC interaction strength mutants, which are labeled as HI ("high degree of interactions"), are PilO(VxxxL) and SadC(T83A); the decreased PilO–SadC interaction strength mutant, which is labeled as LO ("low degree of interactions"), is SadC(L172Q); and wild type (WT) is the baseline strain for comparison. Furthermore, we have the null mutants, which have the genes coding for the key DGCs SadC and/or RoeA deleted and are labeled as NM: Δ*sadC* is the null mutant labeled NM1, and Δ*roeA* Δ*sadC* is the null mutant labeled NM2. We plot the categorized factor scores for each dimension in Figs. 5 and 6. Interestingly,

consistent with data already presented above, the results using lineage data (Figs. 5 *A*–*C* and 6 *A*–*C*) and branch data (Figs. 5 *D*–*F* and 6 *D*–*F*) are again largely consistent with each other.

From the data we can determine how increased or decreased PilO–SadC interaction strength can affect each of the statistically independent contributions to surface commitment at the lineage level. For the dimension corresponding to c-di-GMP mean, compared with WT the HI mutants have lower c-di-GMP mean, while the LO mutant has higher c-di-GMP mean (Fig. 5 *A* and *D*). These results are completely consistent with previous single-cell c-di-GMP results using the same strains (31). Increased PilO–SadC interaction strength correlates with lineages with a smaller c-di-GMP mean and a correspondingly smaller c-di-GMP amplitude in the oscillation. By comparison with the results in the previous section, these lineages tend to detach and have more of their progeny detach (smaller tree symmetry), as seen in Figs. 3 *A* and *D* and 4 *A*, *D*, and *G*. Conversely, decreased PilO–SadC interaction strength correlates with lineages with a larger c-di-GMP mean and a correspondingly larger c-di-GMP amplitude in the oscillation. By comparison, these lineages tend to persist and have more of their progeny persist (larger tree symmetry), as seen in Figs. 3 *A* and *D* and 4 *A*, *D*, and *G*.

Interestingly, modulating PilO–SadC interaction strength in any direction correlates with longer c-di-GMP oscillation periods (Fig. 5 *B* and *E*). Lineages with longer periods tend to detach and have more of their progeny detach, while lineages with shorter periods tend to persist and have more of their progeny persist, as seen in Figs. 3 *B* and *E* and 4 *B*, *E*, and *H*. Finally, for the dimension corresponding to surface motility, compared with WT the HI mutants correlate with lower surface motility, while the LO mutant correlates with higher surface motility (Fig. 5 *C* and *F*). Lineages with lower surface motility tend to persist and have more of their progeny persist, and vice versa, as seen in Figs. 3 *C* and *F* and 4 *C*, *F*, and *I*. We note that the correlation between PilO–SadC interaction strength and surface motility is one of the few cases where lineages and branches have slightly different trends, with the lineage data having a correlation that is not as apparent in the analysis of the branches. One possibility for this discrepancy could be that different branches of a lineage can sample different local environments that can result in heterogeneous surface motility, such that the behavior of the entire lineage does not fully reflect this local environment heterogeneity.

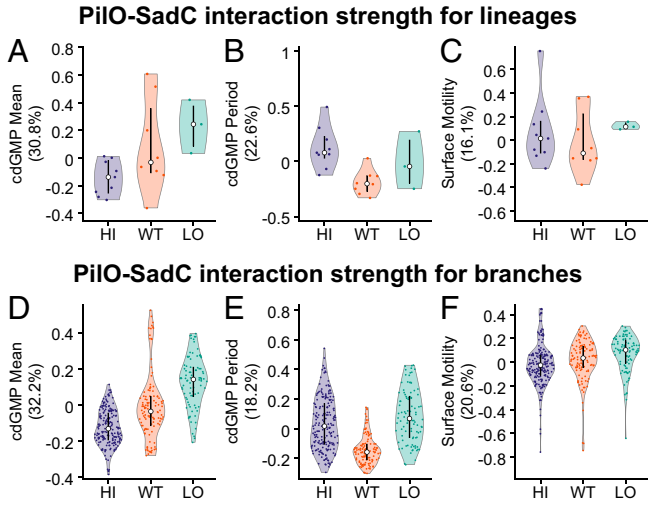

Fig. 5. PilO–SadC interaction strength is optimized for surface commitment. High interaction strength mutants (HI) are PilO(VxxxL) and SadC(T83A), low interaction strength mutant (LO) is SadC(L172Q), and WT is the baseline strain for comparison. (*A* and *D*) Compared with WT, HI mutants have smaller c-di-GMP mean, while LO mutants have larger c-di-GMP mean. In this dimension, having increased interaction strength correlates with higher surface commitment, and vice versa. (*B* and *E*) Compared with WT, all mutants have longer c-di-GMP periods. In this dimension, having a modified interaction strength in any direction correlates with lower surface commitment. (*C* and *F*) Compared with WT, HI mutants have less surface motility, while LO mutants have more surface motility. In this dimension, having increased interaction strength correlates with higher surface commitment, and vice versa. Here, lineages and branches have slightly different trends, with branches having a more apparent correlation. Taken together, these results show that WT has the highest tendency to be surface committed across all dimensions, and either interaction strength mutant is correlated with lower surface commitment in at least one dimension.

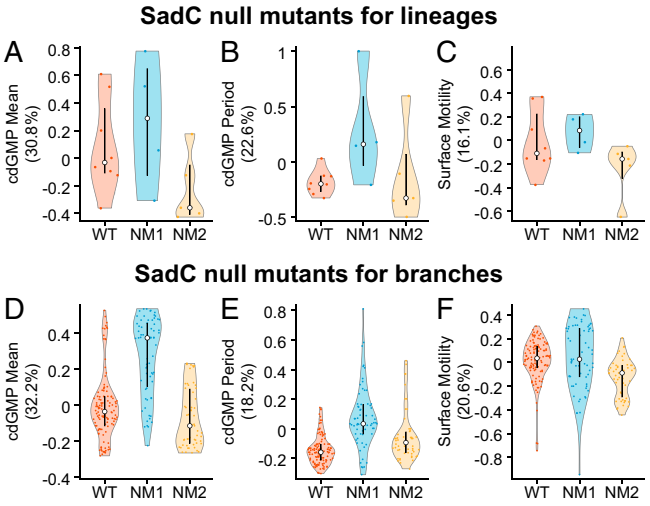

Fig. 6. (*A*–*F*) SadC null mutants show unexpected c-di-GMP trends. The single-null mutant Δ*sadC* (NM1) has counterintuitive results of elevated c-di-GMP levels, large oscillation amplitudes, long oscillation periods, and high surface motility. This mutant behaves very similarly to the LO mutant. The double-null mutant Δ*roeA* Δ*sadC* (NM2) has the expected behavior of a null mutant lacking DGCs, with low c-di-GMP levels, small oscillation amplitudes, short oscillation periods, and low surface motility. WT data are repeated from Fig. 5 for easier comparisons.

We can correlate surface commitment behavior for young bacterial biofilms during the first 10 to 20 generations with specific trends observed for the three FA-derived canonical features. WT lineages do not have decreased tendencies for surface commitment in the dimensions corresponding to mean c-di-GMP levels and surface motility and do have an increased tendency for surface commitment by having shorter c-di-GMP oscillation periods. This observation suggests that WT lineages are characterized by oscillatory c-di-GMP signals that are amplitude- and frequency-modulated in such a way that c-di-GMP levels in a lineage are well-maintained between a minimum and a maximum value for surface commitment. It is interesting to note that the existence of these statistically independent features can allow for conflicting driving forces on cellular behavior, such as values for high mean c-di-GMP levels, large c-di-GMP oscillation periods, and high motility that mandate different surface commitment outcomes and thereby mitigate against one another. It is even more interesting to see how bacteria resolve these conflicts in their behavior, as exemplified by the PilO–SadC interaction mutants. Both PilO–SadC interaction mutants have lineages with decreased tendencies for surface commitment in at least one of the three dimensions. The HI mutants have lineages with lower mean c-di-GMP levels and longer c-di-GMP oscillation periods, which both suggest less surface commitment. However, the HI mutants also have lower surface motility, which suggests more surface commitment. By comparison, the LO mutant has lineages with higher mean c-di-GMP levels, which suggests more surface commitment. However, these LO mutants also have longer c-di-GMP

oscillation periods and higher surface motility, both of which suggest less surface commitment. Adjusting PilO–SadC interaction strength in either direction from baseline WT levels will result in lineages with altered biofilm formation: In both cases, surface commitment is delayed with respect to WT during the first 10 to 20 generations, either through having low mean c-di-GMP levels, so cells never reach the required level, or having elevated c-di-GMP levels that oscillate with large oscillation amplitudes and long periods, which imply a form of dysregulation where cells experience prolonged exposure to alternating low and high c-di-GMP consequences, despite the average level's being elevated. It is important to note that lineages with decreased tendencies for surface commitment in the first 10 to 20 generations do not necessarily lead to less eventual bulk biofilm formation, as c-di-GMP oscillations can potentially enable detached cells to reattach elsewhere. This is the case for the LO mutant, which exhibits large oscillations and does not have significantly less bulk biofilm in crystal violet assays and global c-di-GMP measurements by mass spectrometry despite lower commitment in initial stages of biofilm formation (31). On the other hand, crystal violet assays for the HI mutants do have significantly less biofilm formation, in agreement with early surface commitment trends (31).

The multigenerational lineage analysis above can be extended to the null mutants to resolve apparent contradictions. We find counterintuitive results for the single null mutant Δ*sadC* (NM1), where we observe the lineages with elevated rather than depressed c-di-GMP levels but with large oscillation amplitudes, long oscillation periods, and high surface motility, like that observed in the LO mutant (Fig. 6). Interestingly, the Δ*sadC* null mutant and the LO mutant behave quite differently in bulk c-di-GMP and biofilm crystal violet assays, and these differences could be attributed to SadC's having an additional interaction with the stator, MotC (36). These observations suggest that the effect of a Δ*sadC* deletion is not merely the removal of a DGC and therefore the assumed overall global decrease in c-di-GMP production capacity but a drastic dysregulation of the cells' global c-di-GMP network and the network's compensatory capacity since large-amplitude, large-period c-di-GMP oscillations are observed. Previous work has shown that RoeA is a potential candidate as a compensatory DGC, since SadC and RoeA are known to act in concert during surface sensing (35). Results for the double-null mutant Δ*roeA* Δ*sadC* (NM2) support the hypothesis that RoeA acts as a compensatory DGC in the absence of SadC, where we now observe the expected results of lineages with a drastic decrease in c-di-GMP levels and reduced period and surface motility (Fig. 6).

Together, these null-mutant results provide evidence for how different DGCs can interact with each other in a complex regulatory network. In the case of SadC and RoeA, we find that RoeA apparently overcompensates for the absence of SadC and thereby leads to c-di-GMP signaling dysregulation, given that the Δ*sadC* mutants tend to have lineages with the highest c-di-GMP levels but also lineages with long oscillation periods and large amplitudes that allowed prolonged exposure of cells to low, as well as high, c-di-GMP levels. Finally, there are likely to be other proteins involved, as we do not observe complete absence of c-di-GMP levels even in the double-null mutant.

Discussion

Our findings here paint a more complex and nuanced understanding of cell surface commitment in response to c-di-GMP signaling. By using dimensionality reduction techniques, such as PCA and FA, we can correlate different parameters that characterize c-di-GMP oscillations, including the mean, amplitude, and period, to various quantitative indicators of surface commitment, such as how much of a bacterial lineage persists on the surface. We find that surface commitment in young biofilms is correlated with lineages with elevated c-di-GMP levels and lower surface motility, in agreement with numerous other studies (24, 37, 38). However, we also find that swift surface commitment for the first 10 to 20 generations also correlates with multigenerational oscillating c-di-GMP levels with short (~4 to 6 h) rather than long (~10+ h) oscillation periods. Finally, we find the surprising result that the behaviors exhibited by different individual branches of the family tree are not independent from one another but rather correlated with the collective behavior of the entire multibranched lineage. That is, "family matters" in biofilm formation and appears to facilitate cooperativity in surface commitment behavior. In the time progression of c-di-GMP signals, we note that oscillations clearly appear even when they are averaged across different branches of a lineage, rather than being "washed out" by averaging. This suggests that at least part of the c-di-GMP signal in different branches of a lineage initiated by a single progenitor cell are approximately in phase and thereby contribute to emergence of cooperative surface commitment behavior in a statistical manner (25). The c-di-GMP signal can in principle be impacted by differences in local environmental conditions (such as surface inhomogeneities) experienced by different branches of the lineage. This makes the observation of a persistent common oscillatory c-di-GMP signal across branches of a lineage that propagates from progenitor to progeny all the more striking. In fact, "decoherence effects" can be seen as oscillations gradually become out of phase in different branches, in that cells in more widely separated branches of the family tree tend to behave more differently. An example of this decoherence can be seen in *SI Appendix*, Fig. S1.

In choosing reporter systems for observing real-time behavior in live single cells, we had tried to balance two key considerations in the experimental design. One is the response time of the reporter, which is related to the time lag between the readout (e.g., fluorescence) and the actual activity being reported (e.g., intracellular c-di-GMP levels). The other is the half-life of the fluorophore, which is related to the time lag between the signal's activation and the signal's decay. Both can introduce systematic errors by broadening and distorting the temporal features of the measured fluorescence behavior. Response time contributes to a systematic error in the form of time lag between the readout and the reported activity, while half-life contributes to a systematic error in the form of a time-dependent background signal and a higher baseline level. In general, the longer the response time and/or half-life, the more the errors contribute. For example, by not decaying quickly, the use of a long half-life reporter will enhance the apparent rate of fluorescence signal increase at the beginning of an oscillation and reduce the apparent rate of fluorescence decrease at the end of an oscillation.

The transcriptional reporter used in our experiments works via c-di-GMP binding to FleQ, a transcription factor for the *cdrA* gene; c-di-GMP binding to FleQ causes this transcription factor to dissociate from the *cdrA* promotor and thereby facilitate derepression of *gfp* transcription. One contribution to the noted time lag is the maturation time of the fluorescent protein, which is about 4 min (39). Another contribution to reporter time lag is that associated with c-di-GMP binding to FleQ and derepression of *gfp* transcription. The dynamics of these processes are not as well known but are expected to be significantly less than a division time. We estimate the reporter time lag to be about 10 to 30 min, which is smaller than the time scale of the oscillations, which have a period on the order of about 5 h for WT (with some mutants exhibiting smaller oscillation periods of at least 2 h). We note that GFP half-life can be quite variable from system to system, since protease activity can depend on many factors, such as growth conditions and strain identity (40).* We are currently in the process of obtaining more precise measurements of the

*While we do not expect such protease activity to be c-di-GMP–dependent, we note that even if it were it is not possible to create GFP fluorescence oscillations unless there were c-di-GMP oscillations to begin with.

reporter time lag, which will likely be subject to the intrinsic stochasticity of GFP transcription and translation.

The half-life of the GFP used in the c-di-GMP reporter deserves comment. Our calibration experiments show an estimated reporter half-life of 3.6 ± 1.3 h ($n = 5$) in *P. aeruginosa* PA14 (*SI Appendix*, Fig. S5), which is shorter than reported values in *Escherichia coli* (40). We chose to use a fluorescent protein with a longer half-life so that we could have a higher signal-to-noise ratio and a more stringent test of the existence of oscillations. The long-half-life reporters will tend to be stable longer in the cells and therefore contribute to the signal longer, resulting in a higher signal-to-noise ratio but at the cost of having an increased signal baseline. Moreover, long-half-life reporters will also tend to obscure decreases in c-di-GMP levels. That we observe oscillations in reporter intensity, with clear increases and decreases in signal level, is a strong indication that oscillations in c-di-GMP levels exist. The trade-off is that we expect potentially distortions to the precise line shape of the oscillations.

Finally, we consider how the specific choice of a *cdrA*-based transcriptional reporter influences our results. In our experimental design, we chose to use the plasmid-based *cdrA* transcriptional reporter as an indicator of the presence of c-di-GMP to facilitate comparison with other experiments, in part because it is one of the most widely used reporter systems. This choice of using a *cdrA* transcriptional reporter involved some trade-offs. CdrA is a c-di-GMP–regulated adhesin involved in biofilm formation, and its expression level is unlikely to be constant in time (41). This implies that there can be a changing landscape of competition for c-di-GMP binding between the sensor and natural cellular processes, due to induced changes in *cdrA* expression during biofilm formation, especially those triggered by interactions between bacteria and EPSs, such as Psl (42). Via this competition, we expect monotonic increases in *cdrA* expression to weaken the fluorescence readout rather than generate oscillations. In the extreme scenario of oscillatory *cdrA* expression that is large enough to drive oscillations in the reporter signal via such binding competition, we note that *cdrA* expression is itself regulated by c-di-GMP, so oscillations in *cdrA* expression imply the existence of oscillations in c-di-GMP. Although these potential distortions are difficult to completely eliminate, we have tried to minimize these types of effects by using *P. aeruginosa* PA14 rather than PAO1, which does not leave Psl EPS trails on the surface to interact with other bacteria and thus does not have potential modulation of *cdrA* expression from Psl-induced up-regulation of DGCs and c-di-GMP (42).

It is possible in the future to use different reporter systems: Fluorescence-based reporters are still the main tools for probing real-time dynamics of small molecules in live single cells (43). Besides plasmid-based reporters, other types of reporters include riboswitch- and fluorescence resonance energy transfer (FRET)-based reporters. Riboswitches are regulatory elements of untranslated RNA that can bind ligands such as c-di-GMP and control gene expression. FRET reporters emit a fluorescence signal when the ligand binds and causes a conformational change in the receptor. At present, all of these reporters have trade-offs between response time, signal-to-noise ratio, and dynamic range. Riboswitch and plasmid reporters are expected to have similar issues regarding the time lag of gene expression, while FRET reporters generally have low signal levels and limited dynamic range. Nevertheless, we plan to investigate multigenerational c-di-GMP oscillations using these and new biosensors on the horizon.

The existence of c-di-GMP oscillations that can be amplitude- and frequency-modulated imply that intracellular c-di-GMP levels are maintained between maximal and minimal limits for many generations, likely with ongoing corrections from the cell's c-di-GMP regulatory networks, which in turn depends on how quickly intracellular c-di-GMP levels transduce to c-di-GMP consequences relative to the oscillation period: If the former is slow compared with the latter, then the oscillations will be averaged out and a single uniform population will result. On the other hand, if response to changing c-di-GMP is fast relative to the oscillation period, it is tempting to hypothesize that c-di-GMP oscillation between high and low values can in principle result in a diverse rather than uniform population, guided by a kind of "division of labor" (9) between cells "born" at different parts of a lineage, some with behaviors associated with low c-di-GMP, such as increased motility, and some with behaviors associated with high c-di-GMP, such as increased biosynthesis of EPS. Interestingly, we note a positive statistical correlation between the amplitude of the c-di-GMP oscillation and the mean c-di-GMP level, so that lineages with elevated average c-di-GMP levels tend to have larger oscillation amplitudes, and vice versa, reaching both higher and lower values depending on the size of the oscillation amplitude relative to the average level. This correlation implies that in some lineages there can be forms of amplitude modulation of the c-di-GMP signal that leads to c-di-GMP decreases and forms of c-di-GMP increases that lead to uncontrolled amplitude modulation, both of which can result in potential instability in the biofilm-forming trajectory. Large amplitude oscillations in the c-di-GMP signal can result in extended periods of low c-di-GMP levels even if the mean of that signal is high. These large fluctuations in c-di-GMP levels can be mitigated via another key parameter for surface commitment in the form of the oscillation period: Lineages with elevated c-di-GMP levels and larger oscillation amplitudes can in principle be brought under control by having the c-di-GMP signal be frequency modulated to have a faster feedback response in the cell's regulatory networks governing c-di-GMP levels. Furthermore, unlike the amplitude, the oscillation period is relatively uncorrelated to other parameters, such as the mean c-di-GMP level, so that frequency modulation provides an additional independent level of control on top of amplitude modulation for surface commitment. Indeed, this phenomenon can be observed in the subset of lineages that successfully commit to the surface, which tend to have short oscillation periods in the intracellular c-di-GMP levels. Short c-di-GMP oscillation periods imply that the signal can approach the average quickly no matter what its current value is, thus allowing the cell to respond to large c-di-GMP fluctuations and to have more opportunities to be at the average value. Moreover, having short oscillation periods implies a network fast enough to rapidly respond to environmental or other cues. Our analysis is also consistent with the observations of heterogenous levels of c-di-GMP observed across the population of a single strain when observed at a single-cell level (4, 9, 30, 31, 43–46).

Consistent with the points raised above, we observe that mean c-di-GMP levels and surface motility are not always inversely correlated, which is one of the guiding principles of the present c-di-GMP signaling paradigm (i.e., low mean c-di-GMP and increased surface motility are correlated with lower surface commitment, and vice versa) (24, 37, 38). We see evidence of this phenomenon in the PilO–SadC interaction mutants, which have conflicting independent surface commitment outcomes, such as low mean c-di-GMP and decreased surface motility for the HI PilO–SadC interaction mutants, or high mean c-di-GMP and increased surface motility for the LO mutant. Furthermore, comparing these data with bulk biofilm assays can give some insight into the relative importance of these correlations to surface commitment. Compared with WT, the HI mutants have decreased bulk biofilm formation, while the LO mutant does not have significantly decreased bulk biofilm formation. This comparison suggests that mean c-di-GMP is more important than surface motility for surface commitment, which is consistent with mean c-di-GMP's explaining a larger portion of the total variance of the data. Thus, here we demonstrate not just the importance of c-di-GMP oscillations for surface commitment (statistically ~70% as important as c-di-GMP increases) but also how such oscillations can be

controlled via the important PilO–SadC coupling between T4P and a key hub DGC, as well as how too little or too much PilO–SadC coupling can lead to dysregulation of c-di-GMP amplitude and frequency modulation and thereby impact surface commitment.

Our findings are most striking in the case of SadC, given that the Δ*sadC* mutants tend to have lineages with the highest c-di-GMP levels but with long oscillation periods and large amplitudes that allow prolonged exposure of cells to both high and low c-di-GMP levels. Thus, while some cells in the *sadC* mutant population show high c-di-GMP levels, the dysregulation of the other contributing factors, long oscillation periods and large amplitudes, as well as increased surface motility, contribute to the bulk observation that the Δ*sadC* mutant has a strong biofilm formation defect and lower bulk c-di-GMP levels (31). Finally, our data suggest that the high c-di-GMP levels observed in some Δ*sadC* mutant cells is apparently due to RoeA's overcompensating for the absence of SadC and thereby leads to c-di-GMP signaling dysregulation. In the Δ*sadC* Δ*roeA* double mutant we now observe the expected results of lineages with a drastic decrease in c-di-GMP levels and reduced period and surface motility. Of note, there are likely to be other DGC proteins involved in early signaling, as we do not observe complete absence of c-di-GMP levels even in the double-null mutant. In a more general compass, these results suggest that successful surface commitment and eventual biofilm formation entails precise control of c-di-GMP levels during surface sensing via a complex feedback regulatory network of proteins that include the entire repertoire of DGCs and PDEs.

In support of our findings here, there are multiple reports illustrating examples where behaviors typically associated with increased c-di-GMP levels (i.e., biofilm formation) occur when levels of this dinucleotide remain unchanged or even decrease, and vice versa. For example, studies from the Sauer laboratory showed a transient increase in c-d-GMP levels triggered by the DGC enzyme NicD during dispersion in response to glutamate treatment (47); while c-di-GMP levels eventually drop during dispersion, the initial increase in c-di-GMP is unexpected. The Sauer group also showed that, despite the low level of c-di-GMP found in a strain mutated for the PA3177 gene, the PA3177 mutant strain displays a WT biofilm architecture (48). As another example, a study by Gomelsky and coworkers showed that, as expected, high levels of c-di-GMP promote EPS production, but this results in reduced biofilm formation on plastic (49). Furthermore, the dual domain protein FimX has a degenerate DGC and contested PDE activity; interestingly, a recent publication found that the Δ*fimX* mutant of *P. aeruginosa* produces more EPS but less biofilm biomass than WT over 48 h in a flow cell system (50). With regard to motility, the DGC DgcA is required for gliding motility by *Bdellovibrio bacteriovorus*; the Δ*dgcA* mutant shows decreased global c-di-GMP and is nonmotile because it lacks flagella (51). Furthermore, Alexandre and coworkers showed that a chemotaxis receptor in *Azobacter* enhances motility in response to temporary increases in c-di-GMP. When bound to c-di-GMP, the receptor promotes persistent motility by both increasing swimming velocity and by decreasing swimming reversal frequency (52). Another example can be found in *E. coli*, where c-di-GMP binding to the receptor YcgR, which then binds to the FliG component of the flagellar switch complex, promoting smooth swimming by, again, decreasing swimming reversal frequency (53). Finally, and analogous to our findings here, Sauer and coworkers found that GcbA, a DGC, contributes to reduction of swimming motility, likely via suppression of flagellar reversals without an associated increase in biofilm formation (54). Of course, as we further explore the mechanistic basis of these observations other explanations may come to light, including local-versus-global pools of this second messenger or as-yet-unknown c-di-GMP signaling processes, but we posit that our augmented paradigm for understanding the influence of c-di-GMP present here may explain some of these observations.

Materials and Methods

Strains and Growth Conditions. *P. aeruginosa* PA14 WT and its isogenic strains with point mutations in the *sadC* and *pilO* genes (31) or deletions of the *sadC* and/or *roeA* genes (35) were used in this study. For c di-GMP measurements, a plasmid-based, c-di-GMP–responsive transcriptional reporter, pCdrA::*gfp* (26), was used. Culturing protocols are summarized as follows. Bacteria were plated on lysogeny broth (LB) agar plates and incubated at 37 °C overnight. Individual colonies were swabbed from the plate and grown overnight for ∼18 h in an incubator at 37 °C shaking at 220 rpm. Overnight cultures were regrown in the same overnight growth conditions to an optical density at 600 nm (OD_{600nm}) ∼ 0.4 to 0.6. Regrowth cultures were then diluted in flow cell conditions to an OD_{600nm} ∼ 0.01 to 0.03. These final diluted cultures were used for injection into the flow chamber. Overnight and regrowth media consisted of M63 medium with 1 mM magnesium sulfate, 0.2% glucose, and 0.5% casamino acids (CAA), while flow cell media consisted of M63 medium with 1 mM magnesium sulfate, 0.05% glucose, and 0.125% CAA (4, 34).

Flow Cell Experiments and Data Acquisition. Flow cells were purchased from ibidi (sticky-Slide $VI^{0.4}$ with a glass coverslip) and prepared as previously described (4, 9, 25). The prepared flow cell was connected to a syringe through a 0.22-μm filter (Fisher Scientific) using Silastic silicon tubing of inner diameter 1.57 mm and outer diameter 3.18 mm (Dow Corning) and a natural Kynar poly(vinylidene difluoride) (PVDF) female Luer to 1.6-mm barb adapter (Value Plastics DBA Nordson Medical). An in-line injection port (ibidi) was used at the inlet for inoculating bacteria into the flow cell. Elbow connectors (ibidi) were used to connect the chamber with tubing. The assembled system was flushed with 3% H_2O_2 at a volumetric flow rate of 25 mL/h using a syringe pump (KD Scientific or Harvard Apparatus) and allowed to sit for a total of 4 h including flushing time. The sterilized system was then flushed with autoclaved, deionized water at a flow rate of 5 mL/h using a syringe pump and allowed to sit overnight. Before inoculation of the bacteria into the flow cell, the flow-cell system was flushed with flow-cell medium at 30 mL/h. The diluted bacterial culture was injected into the flow cell and allowed to incubate for 10 to 20 min without flow on the heating stage at 30 °C. Flow was then started at 3 mL/h for the entire acquisition time.

Images were acquired using either an Andor iXon electron-multiplying charge-coupled-device camera with Andor IQ software on an Olympus IX81 microscope equipped with a Zero Drift Correction autofocus system or an Andor Neo scientific complementary metal–oxide–semiconductor camera with Andor IQ software on an Olympus IX83 microscope equipped with a Zero Drift Correction 2 continuous autofocus system. Both systems used a 100× objective, but the IX81 system used an additional 2× lens. Bright-field images were acquired every 3 s or 5 s for the IX81 and IX83 systems, respectively (30-ms exposure time). For c-di-GMP measurements, fluorescence images were also taken every 15 min (500-ms and 150-ms exposure times for the IX81 and IX83 systems, respectively) using a Lambda LS (Sutter Instrument) xenon arc lamp and a GFP filter. The total acquisition time was ∼80 h, resulting in ∼96,000 bright-field images and 320 fluorescence images for each fluorophore. The image size was 67 μm by 67 μm (1,024 by 1,024 pixels) and 133 μm by 133 μm (2,048 by 2,048 pixels) for the IX81 and IX83 systems, respectively.

Lineage Tracking Analysis. Image analysis and lineage tracking were performed in MATLAB R2015a as previously described (4, 9, 25). MATLAB functions from the base installation of MATLAB R2015a, Statistics and Machine Learning Toolbox, Curve Fitting Toolbox, Image Processing Toolbox, Signal Processing Toolbox, and custom MATLAB functions were used for all analyses. In particular, the MATLAB functions "fit" and "pca" were used for function fitting and PCA. A third-party function was used for FA (55), and a third-party package was used for G-causality (27).

Data Availability. Data and scripts used to generate the plots in the figures are available at http://figshare.com (DOI: 10.6084/m9.figshare.17019122) as a single .zip archive file. The data are stored as a MATLAB data file (.mat) called "PlottingData.mat," and the script used to generate the plots is called "PlottingScript.m." The archive file also contains a copy of the custom MATLAB functions needed for generating the plots.

ACKNOWLEDGMENTS. We thank Karin Sauer, Mark Gomelsky, Stefan Kathariosand Chris Waters for providing helpful suggestions regarding c-di-GMP signaling included in the discussion. C.K.L. and G.C.L.W. are supported by the Army Research Office (grant number W911NF-18-1-0254). C.K.L., G.C.L.W., and G.A.O. are supported by the NIH (grant number R01

AI43730). G.A.O. is also supported by the NIH (grant number R37 AI83256). W.C.S. is supported by NSF Graduate Research Fellowships (grant numbers DGE-1650604 and DGE-2034835). J.W.C. is supported by grant number NIH T32 GM 008185, "Systems in Integrative Biology."

1. N. B. Fulcher, P. M. Holliday, E. Klem, M. J. Cann, M. C. Wolfgang, The *Pseudomonas aeruginosa* Chp chemosensory system regulates intracellular cAMP levels by modulating adenylate cyclase activity. *Mol. Microbiol.* **76**, 889–904 (2010).
2. Y. Luo *et al.*, A hierarchical cascade of second messengers regulates *Pseudomonas aeruginosa* surface behaviors. *MBio* **6**, 1–11 (2015).
3. A. Persat, Y. F. Inclan, J. N. Engel, H. A. Stone, Z. Gitai, Type IV pili mechanochemically regulate virulence factors in *Pseudomonas aeruginosa*. *Proc. Natl. Acad. Sci. U.S.A.* **112**, 7563–7568 (2015).
4. C. K. Lee *et al.*, Multigenerational memory and adaptive adhesion in early bacterial biofilm communities. *Proc. Natl. Acad. Sci. U.S.A.* **115**, 4471–4476 (2018).
5. J. W. Hickman, D. F. Tifrea, C. S. Harwood, A chemosensory system that regulates biofilm formation through modulation of cyclic diguanylate levels. *Proc. Natl. Acad. Sci. U.S.A.* **102**, 14422–14427 (2005).
6. Z. T. Güvener, C. S. Harwood, Subcellular location characteristics of the *Pseudomonas aeruginosa* GGDEF protein, WspR, indicate that it produces cyclic-di-GMP in response to growth on surfaces. *Mol. Microbiol.* **66**, 1459–1473 (2007).
7. J. R. O'Connor, N. J. Kuwada, V. Huangyutitham, P. A. Wiggins, C. S. Harwood, Surface sensing and lateral subcellular localization of WspA, the receptor in a chemosensory-like system leading to c-di-GMP production. *Mol. Microbiol.* **86**, 720–729 (2012).
8. V. Huangyutitham, Z. T. Güvener, C. S. Harwood, Subcellular clustering of the phosphorylated WspR response regulator protein stimulates its diguanylate cyclase activity. *MBio* **4**, e00242-00213 (2013).
9. C. R. Armbruster *et al.*, Heterogeneity in surface sensing suggests a division of labor in *Pseudomonas aeruginosa* populations. *eLife* **8**, e45084 (2019).
10. G. O'Toole, H. B. Kaplan, R. Kolter, Biofilm formation as microbial development. *Annu. Rev. Microbiol.* **54**, 49–79 (2000).
11. R. Simm, M. Morr, A. Kader, M. Nimtz, U. Römling, GGDEF and EAL domains inversely regulate cyclic di-GMP levels and transition from sessility to motility. *Mol. Microbiol.* **53**, 1123–1134 (2004).
12. S. S. Branda, S. Vik, L. Friedman, R. Kolter, Biofilms: The matrix revisited. *Trends Microbiol.* **13**, 20–26 (2005).
13. U. Jenal, J. Malone, Mechanisms of cyclic-di-GMP signaling in bacteria. *Annu. Rev. Genet.* **40**, 385–407 (2006).
14. U. Römling, D. Amikam, Cyclic di-GMP as a second messenger. *Curr. Opin. Microbiol.* **9**, 218–228 (2006).
15. U. Römling, R. Simm, Prevailing concepts of c-di-GMP signaling. *Contrib. Microbiol.* **16**, 161–181 (2009).
16. S. Beyhan, F. H. Yildiz, "Cyclic Di-GMP signaling in Vibrio cholerae" in *The Second Messenger Cyclic Di-GMP*, A. J. Wolfe, K. L. Visick, Eds. (ASM Press, 2010), pp. 253–269.
17. C. D. Boyd, G. A. O'Toole, Second messenger regulation of biofilm formation: Breakthroughs in understanding c-di-GMP effector systems. *Annu. Rev. Cell Dev. Biol.* **28**, 439–462 (2012).
18. P. V. Krasteva, K. M. Giglio, H. Sondermann, Sensing the messenger: The diverse ways that bacteria signal through c-di-GMP. *Protein Sci.* **21**, 929–948 (2012).
19. U. Römling, M. Y. Galperin, M. Gomelsky, Cyclic di-GMP: The first 25 years of a universal bacterial second messenger. *Microbiol. Mol. Biol. Rev.* **77**, 1–52 (2013).
20. D.-G. Ha, G. A. O'Toole, "c-di-GMP and its effects on biofilm formation and dispersion: A Pseudomonas aeruginosa review" in *Microbial Biofilms*, M. Ghannoum, M. Parsek, M. Whiteley, P. K. Mukherjee , Eds., (ASM Press, 2015), pp. 301–317.
21. J. K. Teschler *et al.*, Living in the matrix: Assembly and control of *Vibrio cholerae* biofilms. *Nat. Rev. Microbiol.* **13**, 255–268 (2015).
22. M. Valentini, A. Filloux, Biofilms and cyclic di-GMP (c-di-GMP) signaling: Lessons from *Pseudomonas aeruginosa* and other bacteria. *J. Biol. Chem.* **291**, 12547–12555 (2016).
23. K. Sauer, "Cyclic di-GMP and the regulation of biofilm dispersion" in *Microbial Cyclic Di-Nucleotide Signaling*, S.-H. Chou, N. Guiliani, V. T. Lee, U. Römling, Eds. (Springer International Publishing, Cham, Switzerland, 2020), pp. 545–560.
24. S. H. Yoon, C. M. Waters, The ever-expanding world of bacterial cyclic oligonucleotide second messengers. *Curr. Opin. Microbiol.* **60**, 96–103 (2021).
25. C. K. Lee *et al.*, Social cooperativity of bacteria during reversible surface attachment in young biofilms: A quantitative comparison of *Pseudomonas aeruginosa* PA14 and PAO1. *MBio* **11**, e02644-02619 (2020).
26. M. T. Rybtke *et al.*, Fluorescence-based reporter for gauging cyclic di-GMP levels in *Pseudomonas aeruginosa*. *Appl. Environ. Microbiol.* **78**, 5060–5069 (2012).
27. L. Barnett, A. K. Seth, The MVGC multivariate Granger causality toolbox: A new approach to Granger-causal inference. *J. Neurosci. Methods* **223**, 50–68 (2014).
28. C. K. Ellison *et al.*, Obstruction of pilus retraction stimulates bacterial surface sensing. *Science* **358**, 535–538 (2017).
29. I. Hug, S. Deshpande, K. S. Sprecher, T. Pfohl, U. Jenal, Second messenger-mediated tactile response by a bacterial rotary motor. *Science* **358**, 531–534 (2017).
30. B.-J. Laventie *et al.*, A surface-induced asymmetric program promotes tissue colonization by *Pseudomonas aeruginosa*. *Cell Host Microbe* **25**, 140–152.e6 (2019).
31. S. S. Webster, C. K. Lee, W. C. Schmidt, G. C. L. Wong, G. A. O'Toole, Interaction between the type 4 pili machinery and a diguanylate cyclase fine-tune c-di-GMP levels during early biofilm formation. *Proc. Natl. Acad. Sci. U.S.A.* **118**, e2105566118 (2021).
32. N. C. Caiazza, J. H. Merritt, K. M. Brothers, G. A. O'Toole, Inverse regulation of biofilm formation and swarming motility by *Pseudomonas aeruginosa* PA14. *J. Bacteriol.* **189**, 3603–3612 (2007).
33. S. L. Kuchma *et al.*, BifA, a cyclic-Di-GMP phosphodiesterase, inversely regulates biofilm formation and swarming motility by *Pseudomonas aeruginosa* PA14. *J. Bacteriol.* **189**, 8165–8178 (2007).
34. S. L. Kuchma *et al.*, Cyclic-di-GMP-mediated repression of swarming motility by *Pseudomonas aeruginosa*: The *pilY1* gene and its impact on surface-associated behaviors. *J. Bacteriol.* **192**, 2950–2964 (2010).
35. J. H. Merritt *et al.*, Specific control of *Pseudomonas aeruginosa* surface-associated behaviors by two c-di-GMP diguanylate cyclases. *MBio* **1**, e00183-10 (2010).
36. A. E. Baker *et al.*, Flagellar stators stimulate c-di-GMP production by *Pseudomonas aeruginosa*. *J. Bacteriol.* **201**, e00741-00718 (2019).
37. R. Hengge, Principles of c-di-GMP signalling in bacteria. *Nat. Rev. Microbiol.* **7**, 263–273 (2009).
38. R. Hengge, High-specificity local and global c-di-GMP signaling. *Trends Microbiol.* **29**, 993–1003 (2021).
39. E. Balleza, J. M. Kim, P. Cluzel, Systematic characterization of maturation time of fluorescent proteins in living cells. *Nat. Methods* **15**, 47–51 (2018).
40. J. B. Andersen *et al.*, New unstable variants of green fluorescent protein for studies of transient gene expression in bacteria. *Appl. Environ. Microbiol.* **64**, 2240–2246 (1998).
41. B. R. Borlee *et al.*, *Pseudomonas aeruginosa* uses a cyclic-di-GMP-regulated adhesin to reinforce the biofilm extracellular matrix. *Mol. Microbiol.* **75**, 827–842 (2010).
42. Y. Irie *et al.*, Self-produced exopolysaccharide is a signal that stimulates biofilm formation in *Pseudomonas aeruginosa*. *Proc. Natl. Acad. Sci. U.S.A.* **109**, 20632–20636 (2012).
43. A. Petchiappan, S. Y. Naik, D. Chatterji, Tracking the homeostasis of second messenger cyclic-di-GMP in bacteria. *Biophys. Rev.* **12**, 719–730 (2020).
44. M. Christen *et al.*, Asymmetrical distribution of the second messenger c-di-GMP upon bacterial cell division. *Science* **328**, 1295–1297 (2010).
45. C. A. Weiss, J. A. Hoberg, K. Liu, B. P. Tu, W. C. Winkler, Single-cell microscopy reveals that levels of cyclic di-GMP vary among *Bacillus subtilis* subpopulations. *J. Bacteriol.* **201**, e00247-00219 (2019).
46. S. I. Miller, E. Petersen, "Measuring individual cell cyclic di-GMP: Identifying population diversity and cyclic di-GMP heterogeneity" in *Microbial Cyclic Di-Nucleotide Signaling*, S.-H. Chou, N. Guiliani, V. T. Lee, U. Römling, Eds. (Springer International Publishing, Cham, Switzerland, 2020), pp. 193–207.
47. A. Basu Roy, K. Sauer, Diguanylate cyclase NicD-based signalling mechanism of nutrient-induced dispersion by *Pseudomonas aeruginosa*. *Mol. Microbiol.* **94**, 771–793 (2014).
48. B. Poudyal, K. Sauer, The PA3177 gene encodes an active diguanylate cyclase that contributes to biofilm antimicrobial tolerance but not biofilm formation by *Pseudomonas aeruginosa*. *Antimicrob. Agents Chemother.* **62**, e01049-01018 (2018).
49. L.-H. Chen *et al.*, Cyclic di-GMP-dependent signaling pathways in the pathogenic firmicute *Listeria monocytogenes*. *PLoS Pathog.* **10**, e1004301 (2014).
50. Y. M. Cai *et al.*, Differential impact on motility and biofilm dispersal of closely related phosphodiesterases in *Pseudomonas aeruginosa*. *Sci. Rep.* **10**, 6232 (2020).
51. L. Hobley *et al.*, Discrete cyclic di-GMP-dependent control of bacterial predation versus axenic growth in *Bdellovibrio bacteriovorus*. *PLoS Pathog.* **8**, e1002493 (2012).
52. M. H. Russell *et al.*, Integration of the second messenger c-di-GMP into the chemotactic signaling pathway. *MBio* **4**, e00001-00013 (2013).
53. X. Fang, M. Gomelsky, A post-translational, c-di-GMP-dependent mechanism regulating flagellar motility. *Mol. Microbiol.* **76**, 1295–1305 (2010).
54. O. E. Petrova, K. E. Cherny, K. Sauer, The *Pseudomonas aeruginosa* diguanylate cyclase GcbA, a homolog of *P. fluorescens* GcbA, promotes initial attachment to surfaces, but not biofilm formation, via regulation of motility. *J. Bacteriol.* **196**, 2827–2841 (2014).
55. L. Malec, FA. MATLAB Central File Exchange (2007).